

# A quantitative analysis of a multi-phase polycrystalline cubic boron nitride tool material using DualEELS

J. Angseryd<sup>1\*,2</sup>, M. Albu<sup>3</sup>, H-O. Andrén<sup>2</sup>, G. Kothleitner<sup>3</sup>

<sup>1</sup> R&D Sandvik Tooling, SE-126 80 Stockholm, Sweden  
(jenny.angseryd@sandvik.com, +4687266632)

<sup>2</sup> Department of Applied Physics, Microscopy and Microanalysis Group, Chalmers University of Technology, SE-412 96 Gothenburg, Sweden  
(jenny.angseryd@chalmers.se, andren@chalmers.se)

<sup>3</sup> Institute for Electron Microscopy and Fine Structure Research (FELMI), Graz University of Technology, Center for Electron Microscopy, A-8010 Graz, Austria  
(gerald.kothleitner@felmi-zfe.at, mihaela.albu@felmi-zfe.at)

## **Abstract**

This paper presents a quantitative analysis of a polycrystalline cubic boron nitride tool material by electron energy-loss spectroscopy spectrum imaging acquired in dual range mode. Having both the low-loss and core-loss regions acquired nearly simultaneously provides the advantage of accurate corrections for thickness effects and thus the possibility to perform quantification calculations. This has resulted in extracted bonding maps with areal (atoms/nm<sup>2</sup>) or volumetric (atoms/nm<sup>3</sup>) densities. Spectroscopic signatures in the low-loss and core-loss energy ranges, of the elements (Al, B, C, N, Ti and O) present in the existing phases, were studied and used when extracting the element specific bonding maps by the multiple linear least squares fitting procedure. Variations of elemental concentrations across the investigated area were determined, despite of phase overlap in the beam direction or energy overlaps in the EELS spectrum. Moreover, the surface oxidation of Ti(C,N) and AlN as well as the amorphisation of  $\alpha$ -Al<sub>2</sub>O<sub>3</sub> is discussed.

Keywords: TEM, EELS, quantification, ELNES, DualEELS, cBN

## **1 Introduction**

Polycrystalline cubic boron nitride (PCBN) materials are widely used as tool materials in turning operations of hardened steels. This is due to their beneficial mechanical properties like high hardness at high cutting temperatures as well as their higher chemical stability with ferrous materials than for example diamond at the high cutting temperatures [1-4]. PCBN materials usually consist of cubic boron nitride (cBN) grains in a ceramic matrix. In order to optimise PCBN tool material properties it is important to know, in detail, what the microstructure looks like prior to degradation. It is essential to understand the coupling between the microstructure, machining parameters and the degraded microstructure after a machining operation. It is also essential to have the appropriate tools to characterise the microstructure, preferably in a quantitative matter. The applied methodology used in this paper, to extract density maps for all elements in the different phases, is a valuable tool for a quantitative characterisation of this type of complex microstructure.

An overview of the phases in the PCBN material studied here, was obtained in an earlier paper [5] by using energy filtered transmission electron microscopy (EFTEM) and EFTEM spectrum imaging (SI). The first investigations of the same material, degraded after a turning operation, were reported separately [6-7]. The present study is an in-depth characterisation of the PCBN material, focusing on quantitative phase analysis of the matrix phases. An overview of the PCBN material is presented in *figure 1*. cBN grains range from micrometre sized grains to nanometre sized grains in a ceramic matrix. The matrix consists of mainly Ti(C,N) and minor phases such as Al<sub>2</sub>O<sub>3</sub> that are present as a result of reactions taken place during the high-temperature and high-pressure sintering process used to produce these materials.

The material was carefully investigated by using electron energy-loss spectroscopy (EELS) and energy-loss near-edge fine structure (ELNES) measurements in a transmission electron microscope (TEM). With a TEM used in scanning mode (STEM), EELS is a key technique that permits simultaneous studies of the chemical composition and the electronic structure of materials even down to nanometre levels. In order to collect a large data set at once, spectrum imaging can be used. This enables an acquisition of both detailed spatial and spectroscopic information [8-9]. There are several advantages: the entire acquired data set is collected at the same time, under the same running conditions and many processing decisions can be taken after the acquisition itself. On the other hand, in order to optimise the analysis results of the large SI data sets recorded, more advanced off-line processing methods might be needed. Moreover, STEM EELS SI acquired with a new type of spectrometer, the first of which was installed at the FELMI institute in Graz, enables nearly simultaneous acquisition of both low-loss (LL) and core-loss (CL) spectra [10]. The SI can be corrected for energy and spatial drift, and the thickness of the investigated region can be calculated [10-14].

Quantification calculations performed in this study are based on the multiple linear least square (MLLS) fitting procedure [15-16]. The MLLS fitting procedure has commonly been used to resolve energetically closely spaced edges in EELS spectra [17-20], to create bonding maps by for example Arenal et al. [16] as well as to evaluate very low concentrations of trace elements [20]. Extended processing possibilities with spectrum imaging have been demonstrated by Kothleitner and Hofer [21]. STEM EELS SI with “EELS elemental mapping” was utilised in this study and the MLLS separated intensity maps obtained were used in quantification calculations to produce volumetric density maps ( $\text{at}/\text{nm}^3$ ) for each element in the different phases.

While cBN is believed to be stoichiometric, composition variations of the major matrix phase,  $\text{Ti}(\text{C},\text{N})$ , are of great interest and the C/N ratios in different  $\text{Ti}(\text{C}_x\text{N}_{1-x})$  grains were hence studied. Furthermore, the reaction phases present in this PCBN material, i.e.  $\text{Al}_2\text{O}_3$ ,  $\text{TiB}_2$  and  $\text{AlN}$ , were also investigated and quantified. In addition, the influence of surface oxidation on phase identifications and LL effects on the Al  $L_{2,3}$ -edge are discussed. It is also shown that the amorphous  $\text{Al}_2\text{O}_3$  surface layer formed on  $\text{AlN}$  areas can, by means of Al  $L_{2,3}$ -edge and O K-edge ELNES mapping, be differentiated from  $\text{AlN}$ . Spatial distributions of N present in four phases,  $\text{Ti}(\text{C},\text{N})$ , cBN,  $\text{AlN}$  and molecular  $\text{N}_2$ , as well as of oxygen, present in  $\text{Al}_2\text{O}_3$  and also as surface oxide on the  $\text{Ti}(\text{C},\text{N})$  phase, were successfully extracted and quantified.

## 2 *Experimental procedure*

The investigated material is a commercial low content PCBN material, used primarily in hard turning of case hardened steels. The material contains ~55 vol% cBN in a ceramic matrix consisting primarily of  $\text{Ti}(\text{C}_x\text{N}_{1-x})$  and  $\text{Al}_2\text{O}_3$  [5].

### 2.1 *Specimen preparation and experimental equipment*

Thin foil specimens were produced by conventional preparation techniques involving mechanical thinning by spark cutting, grinding and dimpling followed by argon ion milling using a Gatan 691 precision ion polisher system (PIPS).

The analytical investigations were carried out on a FEI Tecnai F20 TEM/STEM (200 kV) equipped with the latest generation of a Gatan imaging filter (GIF Quantum™) with a dual energy range EELS acquisition system. This instrument is a post-column spectrometer and energy-filter that allows nearly simultaneous acquirement of both LL and CL optimised EELS spectra [10-12, 14]. The zero-loss (ZL) peak can be exactly aligned and consequently, after splicing the LL spectra with the CL spectra, energy shifts of the edge onsets can be measured with high precision. A collection semi-angle of 10.8 mrad and a convergence semi-angle of

2.05 mrad were used with a dispersion of 0.3 eV/channel and probe size of ~0.5 nm. Individual acquisition times were applied for the LL spectra and the CL spectra. Typical acquisition times for the data presented in this paper are 0.0024 s for the LL spectra and 0.8 s for the CL spectra. Analysed areas had a relative thickness ( $t/\lambda$ ,  $\lambda$ =electron mean free path) lower than 0.5 with an average relative thickness of 0.3. The system was controlled by Digital Micrograph™ (DM) from Gatan Inc. with the spectrum imaging plug-in, connected to a DigiScan scanning device. Examples of acquired spectra are presented in [figure 2](#).

### 3 Analysis method

#### 3.1 EELS processing and data acquisition procedure

Data from numerous areas in the PCBN material were acquired with STEM/EELS SI and then analysed by a quantification procedure described by Kothleitner et al. [13]. The procedure is based on dual range spectroscopy SI data, where the acquired data sets (LL and CL) are spliced together for energy shift corrections. Quantitative density maps in atoms/nm<sup>3</sup>, with an absolute thickness correction, are obtained with MLLS fitting coefficient maps extracted with ELNES based references.

The spectra in the pixels suffer more or less from a small energy shift relative to each other. Therefore, the data was first corrected by ZL-centring with the Gaussian fitting procedure provided in the Gatan EL/P software. The correction was applied on both the LL SI and the CL SI before they were spliced together by using the splicing option also provided in the Gatan EL/P software. In order to separate closely positioned edges, N-K, Ti-L<sub>2,3</sub> and O-K, and to provide extracted bonding maps the spliced and corrected spectra were processed by the MLLS fitting procedure. By using appropriate ELNES references in the MLLS procedure of a SI, fit-coefficients were returned as fit coefficient maps. [Figure 3](#) shows an example of variations of the ELNES of the N K-edge from cBN, Ti(C,N), AlN and N<sub>2</sub>, which were used in the MLLS fitting procedure to separate the different phases and to obtain coefficient maps. These maps show the spatial distribution of the fitted reference spectra. Areal and volumetric densities of the chemical binding states of each element were calculated by using the relative fit parameters of references integrated over an energy range of 100 eV. Quantification of the extracted maps were performed by using experimental ionisation cross sections for each edge (Al-L<sub>2,3</sub>, B-K, C-K, N-K, Ti-L<sub>2,3</sub> and O-K [22]). Calculated mean free paths [23] for each phase (c-BN, Ti(C<sub>0.7</sub>N<sub>0.3</sub>), TiB<sub>2</sub>, Al<sub>2</sub>O<sub>3</sub> and AlN) together with ZL intensities (also integrated over the 100 eV energy window) and the relative thickness map for the area of interest were used in order to obtain volumetric densities (at/nm<sup>3</sup>), shown in [eq. 1](#).

$$(eq. 1) \quad N_x \left( \frac{at}{nm^3} \right) = \frac{I_x}{I_0 * \sigma_x * \lambda_i * \frac{t}{\lambda_i}}$$

Where  $I_x$  is the edge intensity obtained with a reference of element  $x$  as a fit coefficient map from the MLLS fit;  $I_0$  is the total intensity;  $\sigma_x$  is the experimental cross section;  $\lambda_i$  is the electron mean free path of each phase  $i$  containing element  $x$  and finally  $t$  is the thickness.

The chosen EELS spectral regions were in the ZL-region as well as in the CL-region containing the Al L<sub>2,3</sub>-edge, B K-edge, C K-edge, N K-edge, Ti L<sub>2,3</sub>-edge, O K-edge and Ti L<sub>1</sub>-edge. The MLLS fitting procedure was performed for primarily three distinct energy regions:

1. For Al (70 - 175 eV) with 4 references (Background; LL-reference; Al from Al<sub>2</sub>O<sub>3</sub> and AlN)
2. For B and C (185 - 395 eV) with 5 references (Background; B from cBN and TiB<sub>2</sub>; C from Ti(C,N) and amorphous carbon)
3. For N, Ti and O (395 - 650 eV) with 10 references (Background; N from cBN, Ti(C,N), AlN and N<sub>2</sub>; Ti from Ti(C,N), TiB<sub>2</sub> and Ti L<sub>1</sub>; O from amorphous and  $\alpha$ -Al<sub>2</sub>O<sub>3</sub> as well as Ti(C,N) surface oxide)

Due to the limited dimension of the CCD camera (2048 pixels), the used dispersion (0.3 eV/channel) and the rather low beam current, the simultaneous acquisition of the Al K-edge (1560 eV) was not possible. Additionally, individual background references were used for each region.

Plural scattering effects have a dramatic influence on the ELNES and on the elemental quantification. Fourier deconvolution is possible, but care has to be taken so that computational artefacts do not become error sources for the elemental quantification. Therefore, the SI presented in this work was acquired from regions of mainly 0.3 ( $t/\lambda$ ) relative thicknesses.

### 3.2 Influence from surface oxides

An important issue when working with thin film specimens in TEM with EELS is the tendency of surface oxide formation during specimen preparation or specimen handling. This is especially a problem for specimens with a thickness of less than 100 nm necessary to obtain high EELS signal-to-background ratios. Surface oxides on specimens will influence quantification calculations drastically, especially of oxygen containing phases. In this case oxygen levels are particularly interesting in Al<sub>2</sub>O<sub>3</sub> and as (dissolved) O in Ti(C<sub>x</sub>N<sub>1-x</sub>) as well as in amorphous Al<sub>2</sub>O<sub>3</sub> that occurs when AlN oxidises (*see section 4.3.3*). EELS spectra from other phases occasionally also show an oxygen signal, indicating surface oxidation. These areas were avoided for quantitative analyses. For Ti(C<sub>x</sub>N<sub>1-x</sub>) an oxygen signal was observed in all analysed areas. This can be expected since a small amount of oxygen is assumed to be present in the Ti(C<sub>x</sub>N<sub>1-x</sub>) phase structure, originating from the raw material powder.

### 3.3 Low-loss region influence

Since the Al L<sub>2,3</sub>-edge at 75 eV is used in the MLLS fitting procedure and thus the quantification calculations, it is of great interest to investigate whether LL features can have any influence on this region. Variations of the LL region are observed for the different phases, as seen in *figure 2*. According to Soto [24], the plasmon peak can be used to identify or differentiate between phases like for example TiCN- and TiCNO-films characterised by the main plasmon peak at 23.6 and 25 eV, respectively. Another example is when hexagonal (h)BN is differentiated from cBN by using characteristic features in the plasmon region [25-27]. Differences in the LL regions between the phases (Ti(C<sub>x</sub>N<sub>1-x</sub>), Al<sub>2</sub>O<sub>3</sub>, cBN and TiB<sub>2</sub>) are hence phase characteristic so that it is possible to use them as references in the MLLS fitting procedure to extract phase related maps, as shown in *figure 4a*.

As the EELS spectra acquired from pure Ti(C<sub>x</sub>N<sub>1-x</sub>), cBN and TiB<sub>2</sub> grains show in *figure 2*, features do occur just prior to or in the Al L<sub>2,3</sub>-edge energy region. The impact from Ti-containing phases is dominating. This interference will add additional counts to the Al coefficient map after MLLS fitting, which is observed as Al counts in areas where no Al L<sub>2,3</sub>-edge is found. It will thus also increase the Al content in areas with Al<sub>2</sub>O<sub>3</sub> or AlN, providing quantification calculations with incorrect Al/O and Al/N ratios. An extra reference, in addition to the background reference, was thus used in the MLLS fitting for *region 1*. This is more or less a normalised extracted spectrum, covering the energy-loss for *region 1* (Al

region), from a closely positioned Ti(C,N) grain with comparable thickness. By using this additional reference in the Al L<sub>2,3</sub> region the quality of the fit improved, resulting in correctly extracted intensities for the Al L<sub>2,3</sub>-edge. The LL influence on the Al L<sub>2,3</sub>-edge was especially important for areas with overlapping phases in the beam direction.

## 4 Results

### 4.1 Quantification of the Ti(C<sub>x</sub>N<sub>1-x</sub>) phase - C/N ratio variations

Previous X-ray diffraction investigations [5] of the PCBN material revealed Ti(C<sub>x</sub>N<sub>1-x</sub>) phase peaks showing a mean lattice parameter corresponding to Ti(C<sub>0.7</sub>N<sub>0.3</sub>), assuming stoichiometry and no oxygen content. The XRD peaks were found to be quite wide and EDX as well as EELS showed varying amounts of C and N in different Ti(C<sub>x</sub>N<sub>1-x</sub>) grains, however an unambiguous quantification was not performed. For that purpose, many areas were investigated with EELS STEM SI in this paper.

The Ti L<sub>2,3</sub>-edge shows the characteristic spin-orbit splitting, as the two distinct peaks L<sub>2</sub> and L<sub>3</sub>, [28] in both TiB<sub>2</sub> and Ti(C<sub>x</sub>N<sub>1-x</sub>). The Ti L<sub>2,3</sub>-edge for the two phases appears similar and only small differences are identified. Based on only those two small differences, the MLLS-fit procedure was not able to resolve the two phases. Only one Ti L<sub>2,3</sub> reference was thus used for both TiB<sub>2</sub> and Ti(C<sub>x</sub>N<sub>1-x</sub>). The Ti L<sub>1</sub>-edge, at 564 eV, was also recognised in the selected energy-loss region. A Ti L<sub>1</sub>-edge reference was therefore included in the MLLS processing to remove any contribution to the O K-edge (532 eV).

Examples of quantification of some Ti(C<sub>x</sub>N<sub>1-x</sub>) grains obtained in one SI are presented in [figure 5](#). Primarily two types of Ti(C<sub>x</sub>N<sub>1-x</sub>) grains were identified in this particular area; Ti(C<sub>0.7</sub>N<sub>0.3</sub>) and Ti(C<sub>0.5</sub>N<sub>0.5</sub>). Results from several grains in different acquired SI areas show that the C/N ratio typically varies between 1 and 2.

Individual calculations for Ti, C and N are presented in [figure 6](#) as elemental volumetric distributions for the corresponding binding in the Ti(C<sub>x</sub>N<sub>1-x</sub>) phase, with the grey-scale figures indicating the maximum and minimum quantity (atoms/nm<sup>3</sup>) of an element in the selected areas in that SI area. Quantification details for the mean values of C and N quantities (atoms/nm<sup>3</sup>) and the C/N ratios from four areas, marked as squares in [figure 6](#), are presented here:

- 1) C (36.9 ± 4.6) / N (19.0 ± 3.7) = 1.94
- 2) C (38.0 ± 6.3) / N (18.9 ± 4.6) = 2.01
- 3) C (28.9 ± 4.6) / N (28.7 ± 4.7) = 1.01
- 4) C (29.5 ± 4.9) / N (31.1 ± 5.1) = 0.95

The Ti(C<sub>x</sub>N<sub>1-x</sub>) raw material used in these materials contains some O either in solid solution, a few percent [29], or mainly as surface oxides. The Al added to these materials will react with the surface oxides and form Al<sub>2</sub>O<sub>3</sub> but some O will still be bound in the Ti(C<sub>x</sub>N<sub>1-x</sub>) structure. However, quantitative analyses provide a higher average O content in these grains, ~10 at %. The high O content provided by the quantitative calculation will thus mainly originate from the surface oxide. The Ti(C<sub>x</sub>N<sub>1-x</sub>) phase will therefore inevitably suffer from a phase overlap due to the surface oxidation. At this stage it is not possible to distinguish how much of the O signal that stems from inside the Ti(C<sub>x</sub>N<sub>1-x</sub>) grains and how much that is due to the surface oxide. Only a more in-depth analysis of the fine structure of the specific surface oxide, Ti<sub>x</sub>O<sub>y</sub>, and its thickness estimation would help distinguish between the low O content in the bulk and O from the surface oxide, thus providing more accurate quantification calculations. However, the O K-edge in Ti(C<sub>x</sub>N<sub>1-x</sub>) presents a characteristic ELNES and can at least be separated from the other surface oxides present in this material.

#### 4.2 Quantitative bonding maps for B and N in cBN

cBN is the major phase in this PCBN material, but in this study the matrix phases are in focus. However, several cBN grains were quantified and the results gave, as expected, values for the B/N ratio close to stoichiometry with deviations in the B/N ratio commonly between 1 and 5%. Both the B K-edge and N K-edge in the EELS spectrum have characteristic features and were properly verified with the MLLS fitting procedure. An example of volumetric density maps for B and N in cBN are shown in [figure 4b](#), with minimum and maximum values in  $\text{at}/\text{nm}^3$  corresponding to the grey-scale. An example of the mean volumetric densities values in a selected area of the right cBN grain can be presented as the B/N ratio in  $\text{atoms}/\text{nm}^3$  of  $1.02 (61.3 \pm 1.0 / 60.1 \pm 1.0)$ .

#### 4.3 Quantitative evaluation of PCBN reaction phases $\text{Al}_2\text{O}_3$ , AlN and $\text{TiB}_2$

##### 4.3.1 Oxidation of Al containing phases; $\text{Al}_2\text{O}_3$ and AlN

Aluminium is added to this type of materials in order to react with excess oxygen, originating from surface oxides on the raw material powder, during the high-temperature and high-pressure manufacturing process to avoid any gas formation. Al and O are supposed to react to  $\alpha\text{-Al}_2\text{O}_3$  and form a network between the other grains [5]. The investigations of this PCBN material show  $\text{Al}_2\text{O}_3$  areas and networks in the matrix as well as small areas containing Al and N. These AlN areas were found next to  $\text{Al}_2\text{O}_3$  areas, introducing some problems in the MLLS fitting procedure due to difficulties in the separation between overlapping grains and phases. After comparing the ELNES of Al  $L_{2,3}$ -edges, N K-edges and O K-edges taken from  $\text{Al}_2\text{O}_3$  and AlN areas in the material with other investigations [30-32] three phases were found; namely  $\alpha\text{-Al}_2\text{O}_3$ , AlN and amorphous  $\text{Al}_2\text{O}_3$ . The  $\text{Al}_2\text{O}_3$  in the bulk material has previously been identified as  $\alpha\text{-Al}_2\text{O}_3$  by XRD [5].

##### 4.3.2 Influence of surface oxidation on $\text{Al}_2\text{O}_3$

Normally the Al  $L_{2,3}$ -edge and O K-edge corresponded to those characteristic for  $\alpha\text{-Al}_2\text{O}_3$ . In some  $\text{Al}_2\text{O}_3$  areas, though, a shape difference in the Al  $L_{2,3}$ -edge as well as a shape difference in the peak slope of the O K-edge were observed and identified as amorphous  $\text{Al}_2\text{O}_3$ . This suggests that some  $\alpha\text{-Al}_2\text{O}_3$  areas suffered from amorphisation. Amorphisation can for example be caused by radiation damage during TEM investigations or originate from specimen preparation. However, radiation damage can be identified by a sharp pre-peak on the O K-edge [32], which was never seen in any of the spectra investigated here. This may perhaps be due to the very short acquisition time for each pixel. Consequently, the amorphisation of  $\alpha\text{-Al}_2\text{O}_3$  was in this case assumed to originate from the specimen preparation.

##### 4.3.3 Oxidation states in AlN

EELS spectra taken from AlN regions show variations in the ELNES of both the Al  $L_{2,3}$ -edge and the N K-edge. An additional oxygen signal appeared in all AlN areas studied in this investigation. Differences in both the ELNES of the Al  $L_{2,3}$ -edge and the N K-edge were seen as a function of oxygen content. These variations are connected to the degree of oxidation state of AlN, from a 0-100% oxidised state. The Al  $L_{2,3}$ -edge is smoothed with higher oxidation degree while the N K-edge transforms from a triplet structure within a narrow range to a structure with a dominant first sharp peak [30, 33]. The position of this first sharp peak corresponds to the position of N in molecular form,  $\text{N}_2$  [34-35], which was also found as a single sharp peak in the investigated PCBN specimen. This single sharp N peak was observed in other investigations of oxidised AlN as well [30, 36]. The appearance of O in all AlN areas

in this material indicates some form of surface oxide or O containing AlN phase. In fact, several investigations have reported on AlN and its tendency to spontaneously form surface oxides after specimen preparation [30-31, 33]. Based on the findings from other investigations and ELNES studies of the Al, N and O edges in this study, AlN is assumed to oxidise and form amorphous Al<sub>2</sub>O<sub>3</sub> and additional N<sub>2</sub>. This consequently means that AlN is completely surrounded by Al<sub>2</sub>O<sub>3</sub>, with amorphous Al<sub>2</sub>O<sub>3</sub> located on the surfaces and  $\alpha$ -Al<sub>2</sub>O<sub>3</sub> present as a neighbouring phase in the material.

#### 4.3.4 Quantification of Al containing phases Al<sub>2</sub>O<sub>3</sub> and AlN

In order to illustrate the complexity of extracting quantitative bonding maps for the respective elements in Al<sub>2</sub>O<sub>3</sub> and AlN an acquired SI is evaluated. Al<sub>2</sub>O<sub>3</sub> is mainly found as a network and AlN as small neighbouring areas. Since these two phases often are overlapping, their quantification becomes difficult. The calculations are based on MLLS fitting, done simultaneously over a larger area, by using ELNES references that correspond to the different degrees of oxidation.

In the example shown in [figure 7](#), quantification of the Al-containing phases was intended. Two references for Al were used (one for AlN and one for Al<sub>2</sub>O<sub>3</sub>) as well as an extra LL reference, two references for N (one for AlN and one for N<sub>2</sub>, the N<sub>2</sub> reference is added to be aware of heavily oxidised AlN areas), and either two references for O (one for Al<sub>2</sub>O<sub>3</sub> and one for the amorphous surface oxide) or just one mixed O reference for regions where the separation was suspected to suffer from uncertainties. Additional elemental references from the other phases were of course also included.

The volumetric density maps for Al, N and O, in Al<sub>2</sub>O<sub>3</sub> and AlN, are presented in [figure 7](#). The grey-scale in the density maps indicates the minimum to the maximum value of atoms/nm<sup>3</sup> for the whole SI area. Quantification of a selected area presented in [figure 7](#), with two references for O ( $\alpha$  and amorphous Al<sub>2</sub>O<sub>3</sub>), provided for example a mean O concentration of:  $54.5 \pm 7.2 \text{ atoms/nm}^3$  and a mean Al concentration of:  $38.4 \pm 2.6 \text{ atoms/nm}^3$ , corresponding to an O/Al ratio of 1.42.

Another selected area presented in [figure 7](#) (in the AlN density maps for Al and N) from an oxidised AlN region gives a Al/N ratio (in atoms/nm<sup>3</sup>) of 1.15 ( $9.4 \pm 6.1 / 8.2 \pm 3.3$ ), with large standard deviation values. As previously discussed the AlN areas are surrounded by an amorphous Al<sub>2</sub>O<sub>3</sub> oxide layer with an O/Al ratio of 1.58 ( $47.3 \pm 7.7 / 30.0 \pm 4.2$ ), with large standard deviation values as well. The large deviations are probably related to the influence of oxidation degree on both the Al L<sub>2,3</sub> and the N K-edges.

#### 4.3.5 Quantitative bonding maps for B and Ti in TiB<sub>2</sub>

ELNES variations of the B K-edge were observed in different areas containing TiB<sub>2</sub>. The TiB<sub>2</sub> has a hexagonal, layered-structure with B atoms between Ti atoms. This causes anisotropic bonding that effects ELNES analysis depending on the orientation of grains relative to the direction of the electron beam. It was shown in a separate paper [13] that the fine structure of the B K-edge will vary and that it is possible to separate grains according to their hexagonal axis orientation relative to the beam.

An example of a SI area with two TiB<sub>2</sub> grains is presented in [figure 8](#) with the resulting elemental volumetric density maps in atoms/nm<sup>3</sup> is shown (the values are the minimum and maximum values from the whole SI area). The volumetric density mean values of a selected area in the upper TiB<sub>2</sub> grain provided a B/Ti ratio in atoms/nm<sup>3</sup> of 2.0 ( $44.1 \pm 3.7 / 21.8 \pm 1.0$ ) and a B/Ti ratio for the lower grain in atoms/nm<sup>3</sup> of 1.8 ( $46.2 \pm 5.2 / 25.8 \pm 1.4$ ). The lower grain shows a minor deviation from the parallel orientation with a small impact on the quantification results.

## 5 Discussion

It is shown that surface oxides on specimens as well as other phase overlaps in the beam direction will influence quantification calculations. This especially affects oxygen containing phases, since surface oxidation inevitably induces a phase overlap with implications on the relative thickness and mean free path calculations. For thickness calculations no phase overlap is assumed. Therefore, the deficiency will be reflected in deviations from the nominal absolute volumetric density of each element in each occurring phase. Some density values may hence be lower than the theoretical ones. The mean free path calculations are slightly influenced by the stoichiometry variation. For the Ti(C,N) phase, for example, an average value of the mean free path was used. Nevertheless, despite all error sources significant variations in the C/N ratio from different grains were clearly recognised. The AlN phase both suffered from overlap with another phase (namely amorphous Al<sub>2</sub>O<sub>3</sub>) and local variations in ELNES depending on the degree of oxidation. Quantification of this phase provided low density values, however the ratios corresponded to AlN stoichiometry and it was possible to distinguish the amorphous alumina surface layer. In addition, even though ELNES of the B K-edge varied for the hexagonal TiB<sub>2</sub> it was possible to quantify this phase.

## 6 Conclusions

This study shows that the applied methodology, with element and phase separation with ELNES references as well as quantification with a thickness correction, is appropriate to analyse materials with light elements (B, C, N and O) present in many phases and with grain sizes ranging down to nanometre size (10 nm). It is demonstrated how EELS SIs acquired using dual range spectroscopy in combination with off-line data processing techniques, such as MMLS fitting, can provide a quantitative evaluation of highly complex PCBN type materials. Including absolute thickness measurements in analysed data has provided a tool that can be used to identify microstructure stoichiometry changes as a result of variations in the manufacturing process or after the material has been used as a tool in a machining operation.

An attempt was made to quantitatively analyse the matrix and all reacted phases found in this material. By using ELNES references for the MMLS fitting procedure, experimental cross sections and calculated mean free paths for each stoichiometric phase, quantified elemental bonding maps i.e. volumetric density maps (atoms/nm<sup>3</sup>) were extracted. Several obstacles were identified. Oxidation was concluded to be a major problem especially for Ti(C,N) and AlN which were always found to be oxidised. The small oxygen content of Ti(C,N) could not be quantified because of the amount of surface oxide, but deviations of the C/N ratio in various grains could be determined. For AlN it was possible to differentiate between the core of AlN and the surface oxide, amorphous Al<sub>2</sub>O<sub>3</sub>.

The C/N ratios in the Ti(C<sub>x</sub>N<sub>1-x</sub>) phase differ across the investigated specimen and the stoichiometry most commonly varied between Ti(C<sub>0.5</sub>N<sub>0.5</sub>) and Ti(C<sub>0.7</sub>N<sub>0.3</sub>). Within the experimental error, the measured composition of cBN grains corresponded to stoichiometry. In order to identify the Al containing phases, amorphous and α-Al<sub>2</sub>O<sub>3</sub> as well as AlN, successfully a special background reference was needed in the Al L<sub>2,3</sub>-edge region to extract any influence from the LL region. In addition, extracted phase maps from the LL energy regions were found to correspond very well to extracted bonding maps from the identified phases: TiB<sub>2</sub>, Al<sub>2</sub>O<sub>3</sub>, Ti(C<sub>x</sub>N<sub>1-x</sub>) and cBN.

## Acknowledgments

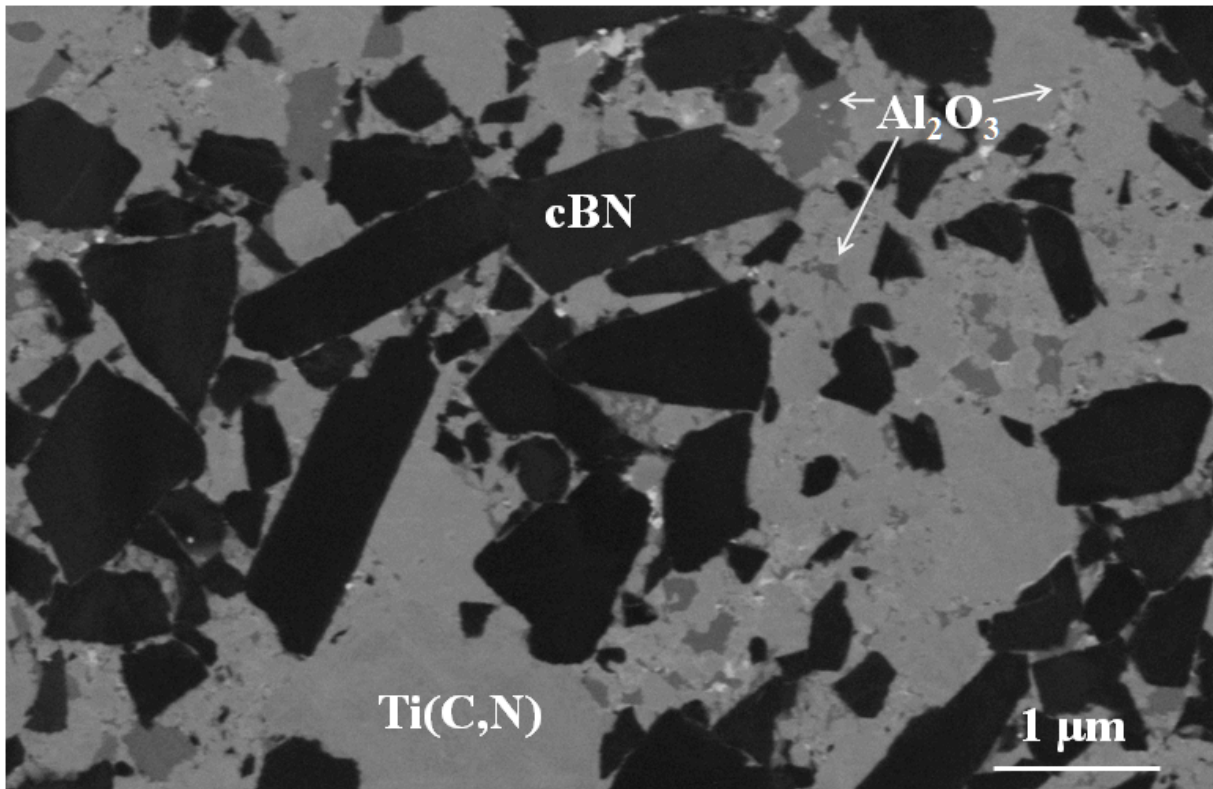
This work was carried out with the financial support by Sandvik Tooling and the Swedish Research Council.

## References

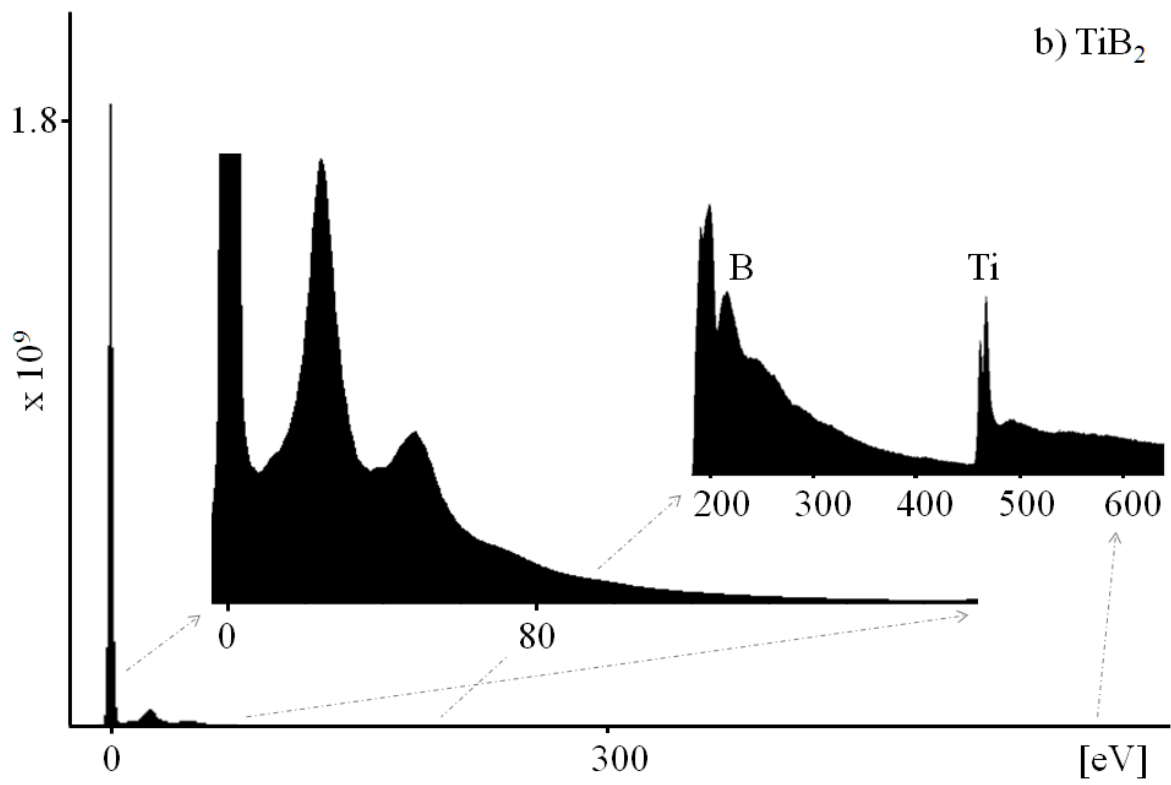
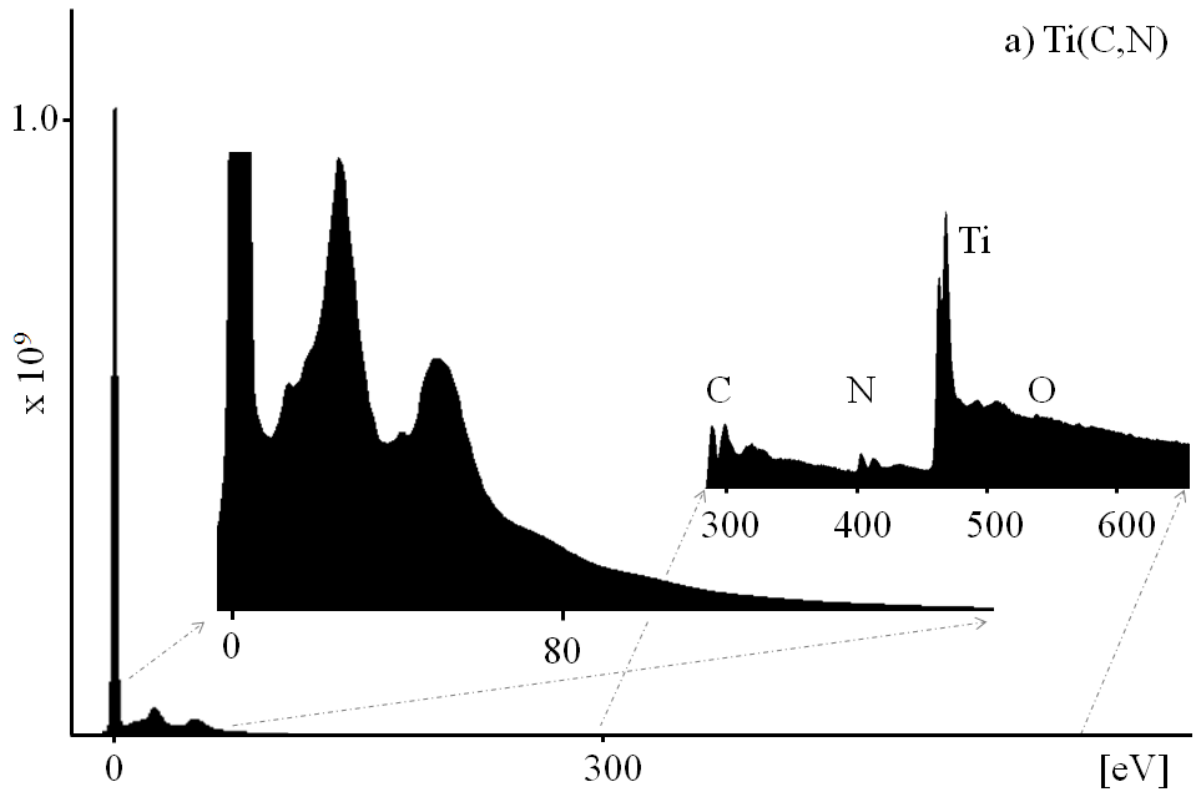
1. R.C. De Vries, *Cubic boron nitride: Handbook of properties*, General Electric Tech. Rep. **6** (1972).
2. P.J. Heath, *Properties and uses of Amborite*, Industrial diamond review. **46** (1986) 120-127.
3. W. König, H.K. Tönshoff, and G. Ackershott, *Machining of Hard Materials*, Annals of the CIRP. **33** (1984) 417-427.
4. C.A. Brookes, *The mechanical properties of cubic boron nitride - a perspective view*, Inst. Phys. Conf. Ser. (1986) 207-220.
5. J. Angseryd, M. Elfving, E. Olsson, and H.-O. Andrén, *Detailed microstructure of a cBN based cutting tool*, International Journal of Refractory Metals and Hard Materials. **27** (2009) 249-255
6. J. Angseryd, E. Coronel, M. Elfving, E. Olsson, and H.-O. Andrén, *The microstructure of the affected zone of a worn PCBN cutting tool characterised with SEM and TEM*, Wear. **267** (2009) 1031-1040.
7. J. Angseryd and H.-O. Andrén, *An in-depth investigation of the cutting speed impact on the degraded microstructure of worn PCBN cutting tools*, Accepted for publication in Wear.
8. J.A. Hunt and D.B. Williams, *Electron energy-loss spectrum-imaging*, Ultramicroscopy. **38** (1991) 47-73
9. C. Jeanguillaume and C. Colliex, *Spectrum-image: The next step in EELS digital acquisition and processing* Ultramicroscopy **28** (1989) 252-257
10. A. Gubbens, M. Barfels, C. Trevor, R. Twesten, P. Mooney, P. Thomas, N. Menon, B. Kraus, C. Mao, and B. McGinn, *The GIF Quantum, a next generation post-column imaging energy filter*, Ultramicroscopy. **110** (2010) 962-970
11. M. Tencé, T. Birou, C. Lopez, and C. Pertel, *Towards systematic single scattering EELS analysis with improved energy resolution. A new detection scheme.*, EDGE meeting 2009 proceedings. (2009) 65.
12. J. Scott, P.J. Thomas, M. MacKenzie, S. McFadzean, J. Wilbrink, A.J. Craven, and W.A.P. Nicholson, *Near-simultaneous dual energy range EELS spectrum imaging*, Ultramicroscopy. **108** (2008) 1586-1594
13. G. Kothleitner, M. Albu, and J. Angseryd, *Towards more quantitative electron energy-loss spectroscopy by nearly simultaneous acquisition of low and high losses*, In manuscript.
14. G. Kothleitner and P.J. Thomas, *Accurate chemical shift measurements using a post-column spectrometer equipped with an experimental shutter*, EDGE meeting 2009 proceedings. (2009) 62.
15. M. Tencé, M. Quartuccio, and C. Colliex, *PEELS compositional profiling and mapping at nanometer spatial resolution* Ultramicroscopy. **58** (1995) 42-54.
16. R. Arenal, F. de la Peña, O. Stéphan, M. Walls, M. Tencé, A. Loiseau, and C. Colliex, *Extending the analysis of EELS spectrum-imaging data, from elemental to bond mapping in complex nanostructures*, Ultramicroscopy. **109** (2008) 32-38
17. M. Albu, F.M. Martín, G. Kothleitner, and B. Sonderegger, *Compositional characterisation and thermodynamic modelling of nitride precipitates in a 12% Cr steel* International Journal of Materials Research. **99** (2008) 422-427
18. P. Harkins, M. MacKenzie, A.J. Craven, and D.W. McComb, *Quantitative electron energy-loss spectroscopy (EELS) analyses of lead zirconate titanate*, Micron. **39** (2009) 709-716.
19. R.D. Leapman and C.R. Swyt, *Separation of overlapping core edges in electron energy loss spectra by multiple-least-square fitting*, Ultramicroscopy. **26** (1988) 393-404.
20. K. Riegler and G. Kothleitner, *EELS detection limits revisited: Ruby - a case study*, Ultramicroscopy. **110** (2010) 1004-1013.
21. G. Kothleitner and F. Hofer, *Elemental occurrence maps: a starting point for quantitative EELS spectrum image processing* Ultramicroscopy. **96** (2003) 491-508
22. F. Hofer, *Determination of inner-shell cross-sections for EELS quantification*, Microsc. Microanal. Microstruct. **2** (1991) 215-230.
23. T. Malis, S.C. Cheng, and R.F. Egerton, *EELS Log-Ratio Technique for Specimen-Thickness Measurement in the TEM*, Journal of Electron Microscopy Technique. **8** (1988) 193-200.
24. G. Soto, *AES, EELS and XPS characterization of Ti(C, N, O) films prepared by PLD using a Ti target in N<sub>2</sub>, CH<sub>4</sub>, O<sub>2</sub> and CO as reactive gases* Applied Surface Science. **233** (2004) 115-122
25. E. Weißmantel, T. Pfeifer, and F. Richter, *Electron microscopic analysis of cubic boron nitride films deposited on fused silica*, Thin Solid Films. **408** (2002) 1-5.
26. D.R. McKenzie, D.J.H. Cockayne, D.A. Muller, M. Murakawa, S. Miyake, S. Watanabe, and P. Fallon, *Electron optical characterization of cubic boron nitride thin films prepared by reactive ion plating* Journal of Applied Physics **70** (1991) 3007-3012.
27. M. Lattemann, S. Ulrich, and J. Ye, *New approach in depositing thick, layered cubic boron nitride coatings by oxygen addition—structural and compositional analysis*, Thin Solid Films. **515** (2006) 1058-1062

28. D.B. Williams and C.C. Carter, *Transmission Electron Microscopy*. 1996, New York: Springer Science+Business Media, LLC.
29. J. Angseryd, F. Liu, H.-O. Andrén, S.S.A. Gerstl, and M. Thuvander, *Quantitative APT analysis of Ti(C,N)*, Accepted for publication in *Ultramicroscopy*, <http://dx.doi.org/10.1016/j.ultramic.2011.01.031>.
30. M. MacKenzie and A.J. Craven, *Quantifying the oxidation of AlN using electron energy loss spectroscopy* *Journal of Physics D: Applied Physics*. **33** (2000) 1647-1655
31. M. Sternitzke, *Growth of Oxide Layers on Thin Aluminium Nitride Samples Measured by Electron Energy-Loss Spectroscopy*, *Journal of American Ceramic Society*. **79** (1993) 2289-2294.
32. D. Bouchet and C. Colliex, *Experimental study of ELNES at grain boundaries in alumina: Intergranular radiation damage effects on Al-L<sub>2,3</sub> and O-K edges* *Ultramicroscopy*. **96** (2003) 139-152.
33. V. Serin, C. Colliex, R. Brydson, S. Matar, and F. Boucher, *EELS investigation of the electron conduction-band states in wurtzite AlN and oxygen-doped AlN(O)*, *Physical Review B*. **58** (1998) 5106-5115.
34. R. McLaren, S.A.C. Clark, I. Ishii, and A.P. Hitchcock, *Absolute oscillator strengths from K-shell electron-energy-loss spectra of the fluoroethenes and 1,3-perfluorobutadiene* *Physical Review A*. **36** (1987) 1683-1701.
35. S. Trasobares, O. Stéphan, C. Colliex, G. Hug, W.K. Hsu, H.W. Kroto, and D.R.M. Walton, *Electron beam puncturing of carbon nanotube containers for release of stored N<sub>2</sub> gas* *European Physical Journal B*. **22** (2001) 117-122.
36. J. Chaudhuri, L. Nyakiti, R.G. Lee, Z. Gu, J.H. Edgar, and J.G. Wen, *Thermal oxidation of single crystalline aluminum nitride*, *Materials Characterization*. **58** (2007) 672-679.

*Figures:*



**Figure 1.** An in-lens backscatter SEM micrograph of the PCBN material. The major phases are indicated in the micrograph, i.e. cBN and Ti(C,N) as well as Al<sub>2</sub>O<sub>3</sub>. Small white areas correspond to WC, present in the material from milling bodies in the manufacturing process [5].



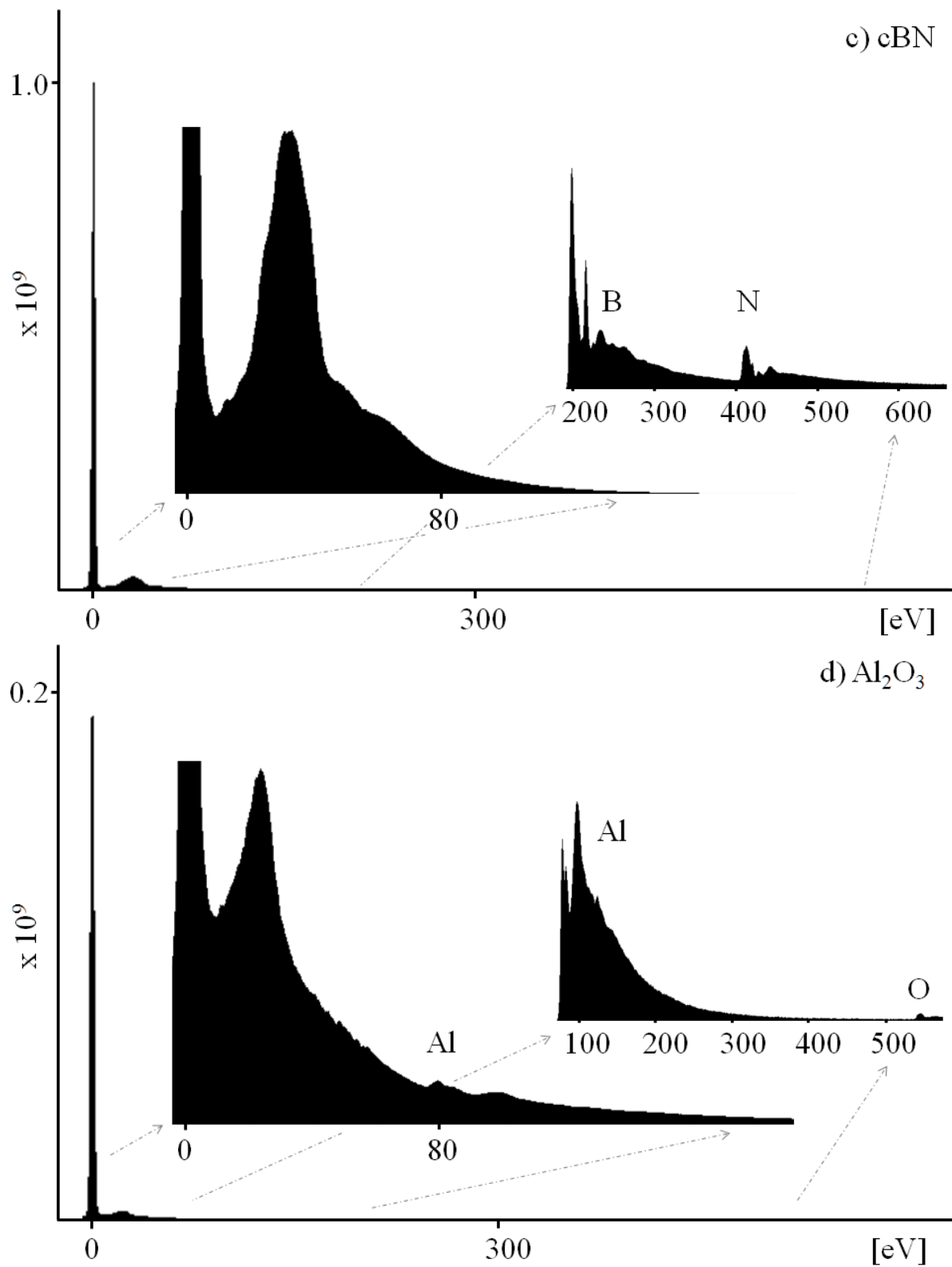


**Figure 2.** EELS spectra with the ZL peak, the low-loss regions as well as the core-loss edges from **a)**  $\text{Ti}(\text{C}_x\text{N}_{1-x})$ , **b)**  $\text{TiB}_2$  **c)** cBN and **d)**  $\text{Al}_2\text{O}_3$ . The low-loss region is especially interesting because of its impact on the Al  $L_{2,3}$ -edge as discussed in [section 3.3](#).

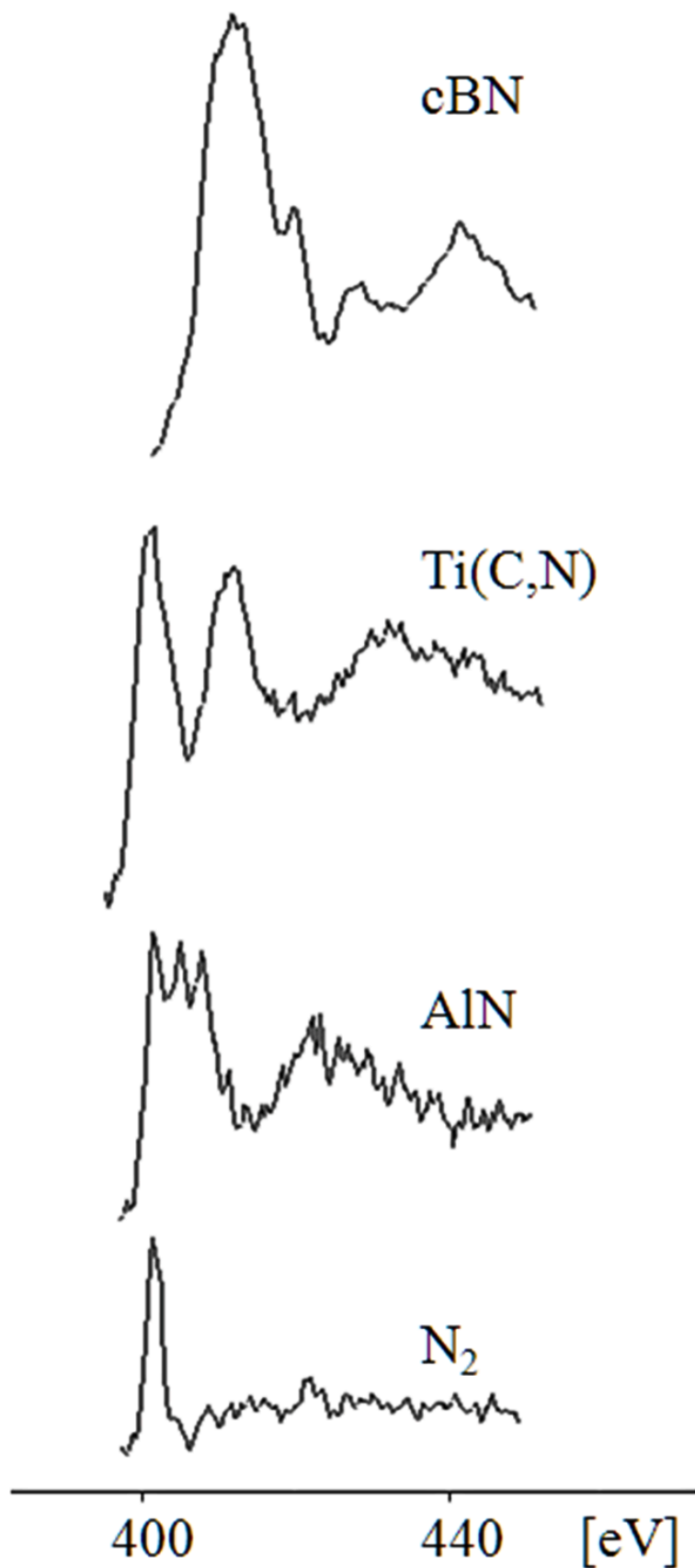


**Figure 3.** ELNES of the N K-edge in cBN, Ti(C,N), AlN and N<sub>2</sub>. The local variations of the edge are used to separate N containing phases with the MLLS fitting procedure and to extract phase coefficient maps used in quantification calculations.

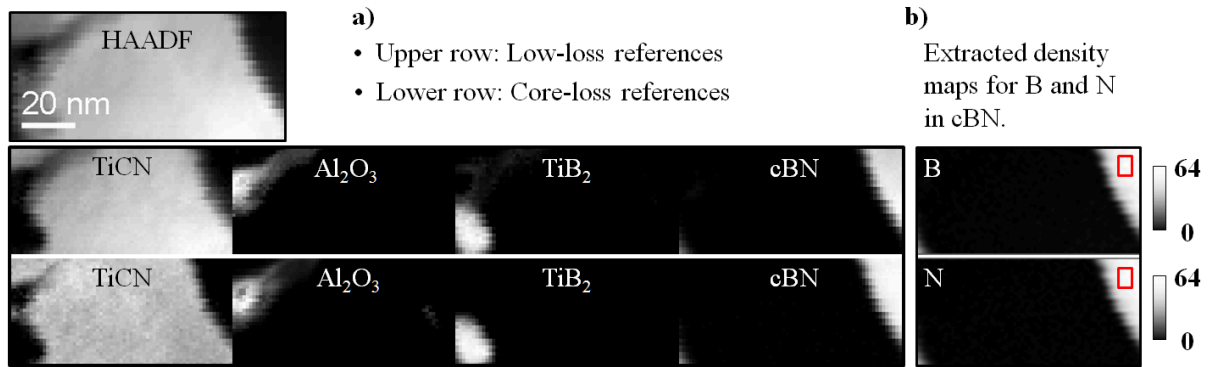


**Figure 4. a)** A HAADF STEM image, acquired during the SI, and MLLS extracted bonding maps from  $\text{Ti}(\text{C}_x\text{N}_{1-x})$ , cBN,  $\text{Al}_2\text{O}_3$  and  $\text{TiB}_2$ . The upper maps are calculated with references from the low-loss region (8-108 eV) and the lower maps with core-edge references (Ti  $L_{2,3}$ -edge for  $\text{Ti}(\text{C}_x\text{N}_{1-x})$ , separate B K-edge for cBN and  $\text{TiB}_2$  as well as O K-edge for  $\text{Al}_2\text{O}_3$ ). **b)** The B and N volumetric density bonding maps for cBN with the maximum and minimum values (atoms/ $\text{nm}^3$ ) from the whole SI area. Even though only a part of a larger cBN grain is visible in this specific SI area, it is a good example since there are no overlaps with other grains. The red squares indicate the areas quantified in [section 4.2](#).

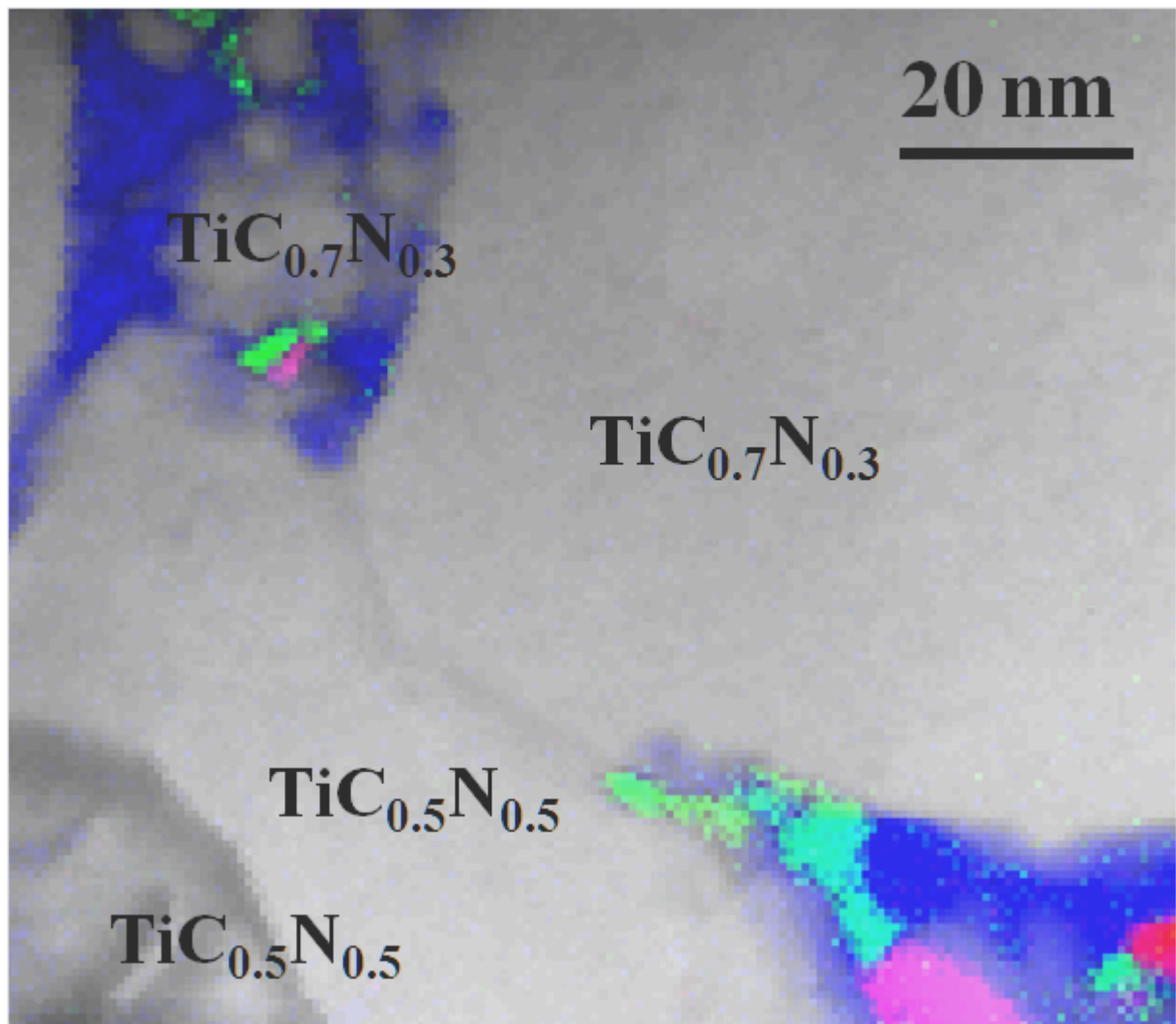


**Figure 5.** Colour map of an area with  $\text{Ti}(\text{C}_x\text{N}_{1-x})$  (white/grey) grains with different C/N ratio as well as areas of  $\text{Al}_2\text{O}_3$  (blue), AlN (light green),  $\text{TiB}_2$  (pink) and cBN (red). This area is presented as density maps in [figure 5](#).

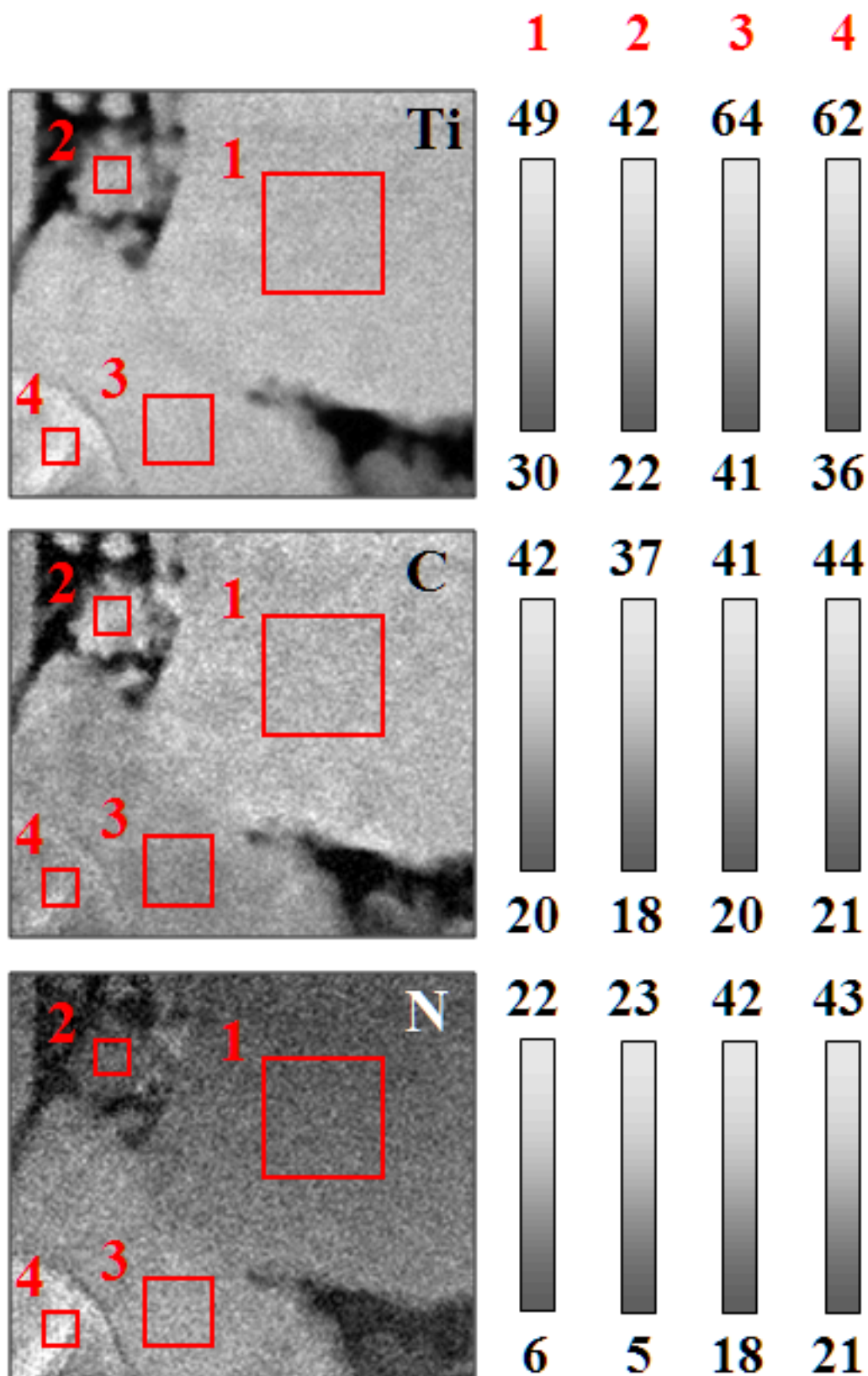


**Figure 6.** Extracted quantitative bonding maps for Ti, C and N from the area also shown in *figure 4*. The grey-scale figures the maximum and minimum quantity (atoms/nm<sup>3</sup>) of each element obtained from the marked squares in the SI area. EELS data from the red squares are used in the quantification calculations in *section 4.1*.

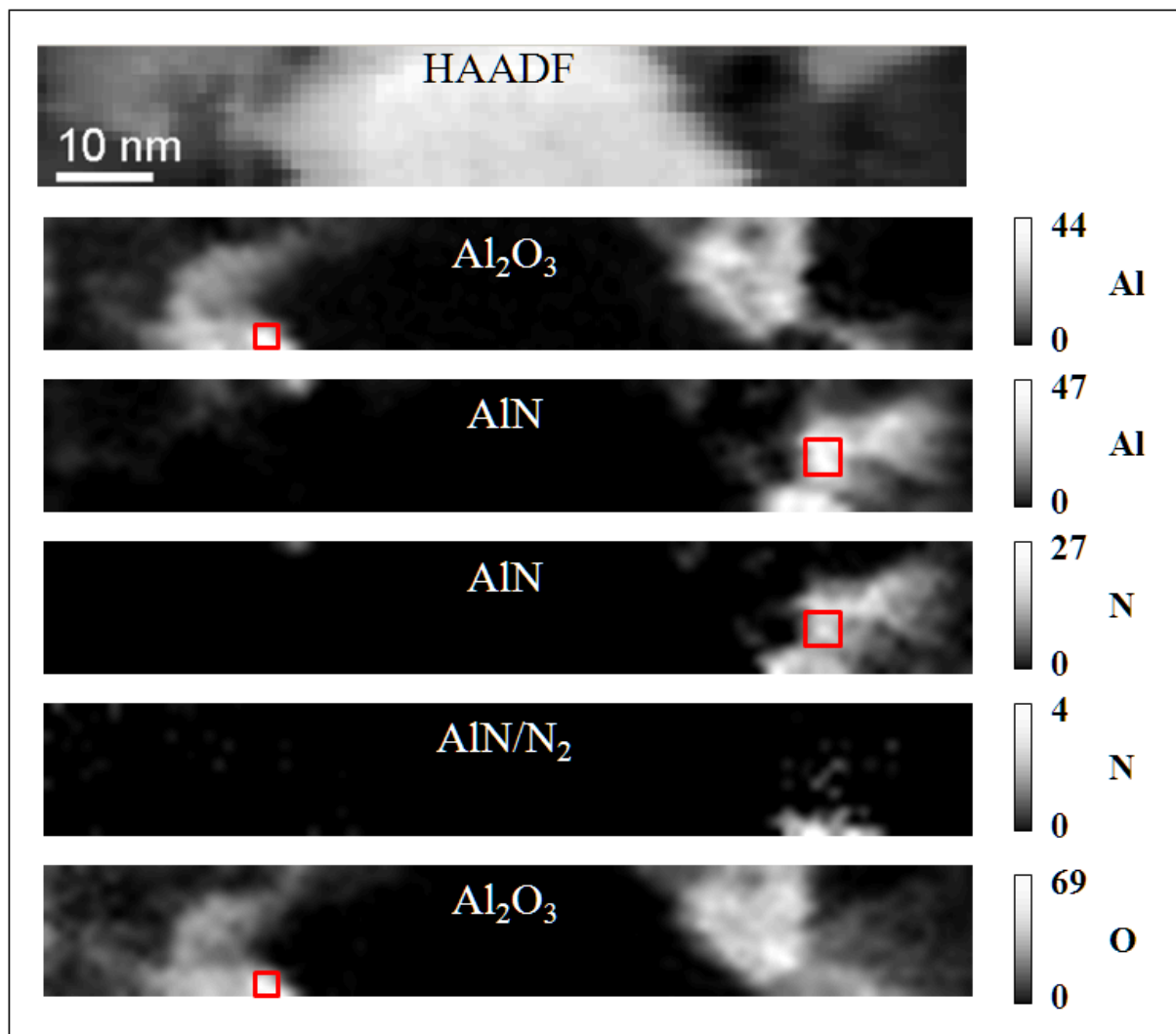


**Figure 7.** A HAADF STEM image, acquired during the SI, as well as the spatial distribution (as specific volumetric density maps) presented for Al, N and O atoms in Al<sub>2</sub>O<sub>3</sub> and AlN. The influence of the amorphous Al<sub>2</sub>O<sub>3</sub> surface oxide layer is included in the Al maps and the O map. N signal originating from the molecular N K-edge is presented in a separated map, AlN/N<sub>2</sub>. The maximum and minimum amounts (atoms/nm<sup>3</sup>) from the whole SI area are indicated. EELS data from the red squares are used in the quantification of mean values in [section 4.3.4](#). TiB<sub>2</sub> grains found in this area are shown and quantified in [figure 7](#).

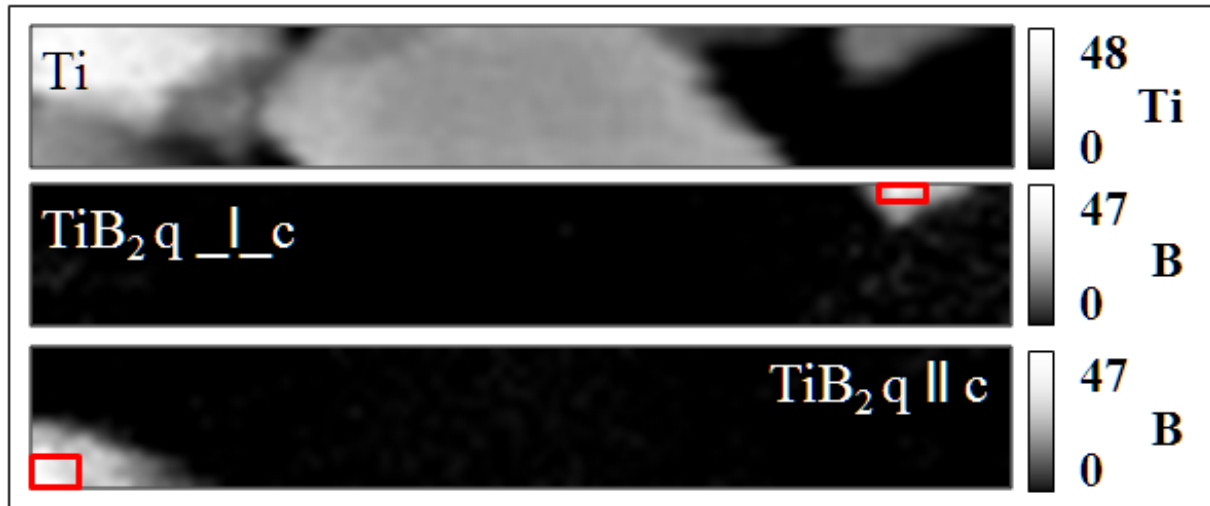


**Figure 8.** Orientation dependent volumetric densities (atoms/nm<sup>3</sup>) for TiB<sub>2</sub>, from the same area as shown in *figure 6*. The gray scale represents the minimum and maximum values from the whole SI area (at/nm<sup>3</sup>). The Ti map also includes signal from Ti(C,N) (a large Ti(C,N) grain is found in the centre and in the upper left corner). The red squares indicate the selected areas quantified in [section 4.3.5](#).